Journal of Asian Earth Sciences 37 (2010) 384–393

Contents lists available at ScienceDirect

Journal of Asian Earth Sciences

journal homepage: www.elsevier.com/locate/jseaes

Zircon U–Pb geochronology, Sr–Nd isotope analyses, and petrogenetic study of the Dehnow diorite and Kuhsangi granodiorite (Paleo-Tethys), NE Iran

M.H. Karimpour [a,*], C.R. Stern [b], G.L. Farmer [b]

[a] Research Center for Ore Deposit of Eastern Iran, Ferdowsi University of Mashhad, Iran
[b] Department of Geological Sciences, University of Colorado, CB-399, Boulder, CO 80309, USA

ARTICLE INFO

Article history:
Received 13 May 2009
Received in revised form 22 October 2009
Accepted 9 November 2009

Keywords:
Mashhad
Iran
Paleo-Tethys
Ilmenite series
Rb–Sr
Sm–Nd
U–Pb–zircon

ABSTRACT

The Paleo-Tethys ocean opened in Silurian time, and its subduction under the Turan plate started in the Late Devonian. By Late Triassic time (225 Ma), no Paleo-Tethys crust remained on the surface of the Iranian plate. Subsequently, however, obduction of the Turan plate over the Iranian plate emplaced allochthonous sheets in what is now northeastern Iran. The sheets contain meta-ophiolites, which have been dated at 281.4 and 277.4 Ma by the ^{40}Ar–^{39}Ar method. These remnant Paleo-Tethys meta-ophiolites and associated metaflysch sequences were intruded by the Dehnow diorite and Kuhsangi granodiorite. Zircon U–Pb dating indicates that the age of the Kuhsangi granodiorite is 217 ± 4 Ma and that of the Dehnow diorite is 215 ± 4 Ma (Late Triassic, Norian). The granodiorite and diorite have magnetic susceptibilities of between 5×10^{-5} and 20×10^{-5} (SI units) and therefore are classified as belonging to the ilmenite series of reduced-type granitoids. Chemically, the Dehnow diorite and Kuhsangi granodiorite are moderately peraluminous S-type plutons with $(La/Yb)_N$ = 7–22 and no, or only small, negative Eu anomalies ($Eu/Eu* = 0.55–1.1$). Their initial $^{87}Sr/^{86}Sr$ ratios range from 0.707949 to 0.708589, and their initial ε_{Nd} values range from −6.63 to −5.90 when recalculated to an age of 216 Ma. These values could be considered to represent continental crust–derived magmas, and metagreywacke to metapelite with initial ε_{Nd} values of −15.01 may have been involved in their genesis, but these were not the sole parent material.

1. Introduction

The study area is within the Binaloud Mountains, south and west of Mashhad city in northeastern Iran, between Longitude 59°23′55″E to 59°33′41″E and Latitude 36°16′19″N to 36°22′55″N (Fig. 1). The Binaloud Mountains include meta-ophiolites and metaflysch sequences interpreted as remnants of the Paleo-Tethys ocean. These rocks are intruded by diorite and granodiorite plutons.

Previous geologic studies in the Binaloud region include mineral reconnaissance on the granite and diorite plutons, meta-ophiolites, and metasedimentary rocks (Jarchovski et al., 1973). The earliest petrographic study of the Mashhad granites was carried out by Alberti and Moazez (1974). Majidi (1983) did a Ph.D. thesis on the meta-ophiolite and the metamorphic and granitic rocks, and Mirnejad (1991) wrote a M.Sc. thesis on the petrography and major element contents of the intrusive rocks. Alavi (1979, 1991, 1992) studied the structural characteristics of the area in detail. Valizadeh and Karimpour (1995) performed a petrographic and major element study of the granitoids. Iranmanesh and Sethna (1998) investigated the Mashhad granites. Abbasi (1998) did his M.Sc. project on both regional and contact metamorphic rocks. Ghazi et al. (2001) studied the geochemistry and determined the age of the Mashhad meta-ophiolite.

The Dehnow–Kuhsangi study area is the only exposure of Paleo-Tethys granitoid rocks in Iran. Our research in the area during more than 10 years has shown that the K-Ar ages of 256–245 Ma determined for the Dehnow–Kuhsangi granitoids by Majidi (1983) are older than their stratigraphic age, as indicated by crosscutting relationships. Our work also shows that the interpretation made by Iranmanesh and Sethna (1998) that the Dehnow and Kuhsangi diorite and granodiorite are I-type granites belonging to the magnetite series is incorrect. Here we present the results of new radiogenic isotope analysis and more accurate zircon U–Pb dating. We then discuss the paleotectonic and petrogenetic implications of these new data for the Paleo-Tethys Dehnow–Kuhsangi granitoids.

2. Geological setting

The Binaloud region in northeastern Iran, south of Mashhad, contains Paleo-Tethys remnants, including the Dehnow diorite and Kuhsangi granodiorite. To the west, such remnants extend into the Alborz Mountains and then to Azerbaijan, Armenia, Turkey, and

* Corresponding author. Address: Research Center for Ore Deposit of Eastern Iran, Ferdowsi University of Mashhad, P.O. Box No. 91775-1436 Mashhad, Iran. Tel./fax: +98 0511 8797275.
E-mail address: mhkarimpour@yahoo.com (M.H. Karimpour).

1367-9120/$ - see front matter © 2009 Elsevier Ltd. All rights reserved.
doi:10.1016/j.jseaes.2009.11.001

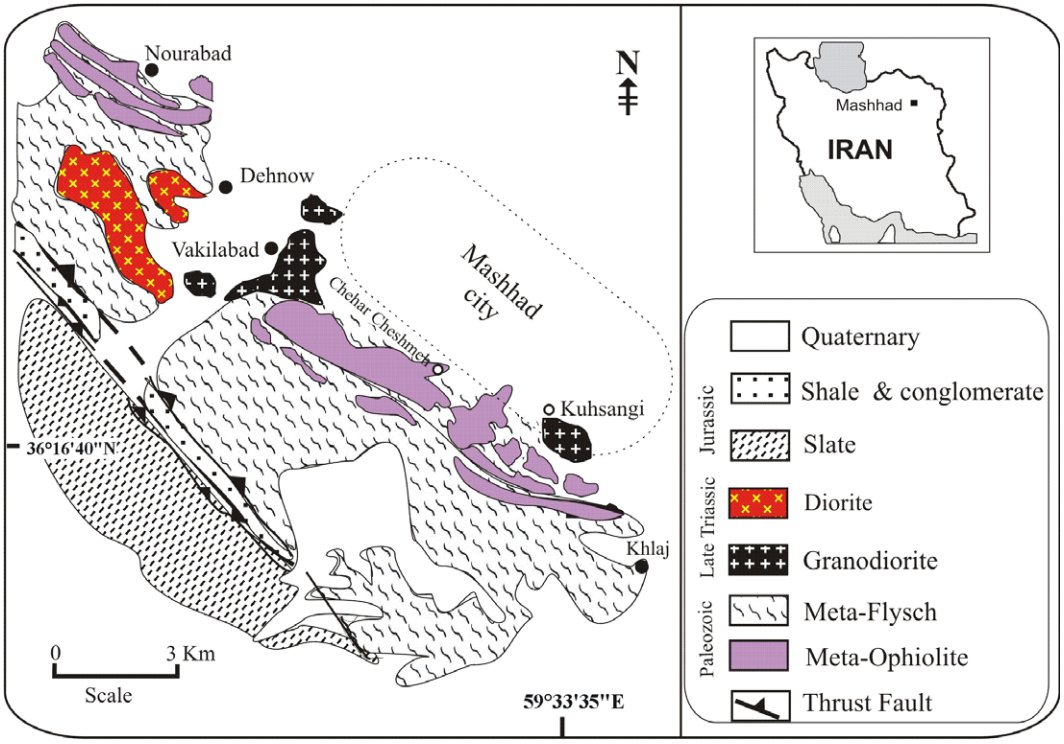

Fig. 1. Geological location of Kuhsangi granodiorite and Dehnow diorite.

other parts of Europe. To the east, they extend to the Hindu-Kush Mountains north of Afghanistan and India.

The Dehnow diorite and Kuhsangi granodiorite were formed during the collision of the Iranian and Turan plates. These granitoids intruded the meta-ophiolite and metaflysch Paleo-Tethys remnants. They are the only exposure of the Paleo-Tethys granitoid rocks in Iran.

During the Paleozoic, the Iranian and Arabian plates formed a coherent unit and were separated from the Turan plate by the Paleo-Tethys. The research of Stampfli (1996, 2000, 2002); Stampfli and Pillevuit (1993), and Stampfli et al. (1991) in the Alborz Mountains and elsewhere has yielded very good evidence that the Paleo-Tethys ocean opened in Silurian time. In the late Paleozoic or Early Triassic, the Iranian plate drifted away from Arabia as the Neo-Tethys ocean opened, and the Iranian microcontinent collided with the Turan plate. In Iran, Turkey, and Greece, the Paleo-Tethys closure occurred during the Late Triassic (between 231 and 225 Ma). By the end of the Late Triassic, the closure of the Paleo-Tethys was complete in the area that would become Iran (Stampfli, 1996, 2002; Stampfli and Pillevuit, 1993; Stampfli et al., 1991; Davoudzadeh and Schmidt, 1984).

The obduction of the Paleo-Tethys meta-ophiolite and metaflysch and their emplacement over the Iranian microcontinental margin must have been Pre-Late Triassic (Stampfli, 1996, 2002; Stampfli and Pillevuit, 1993; Stampfli et al., 1991; Davoudzadeh and Schmidt, 1984; Alavi, 1992). Alavi (1992) and Stocklin (1974) also concluded that the initiation of the collisional processes between the Iranian microcontinent and the Turan plate had been started prior to the end of Triassic.

2.1. Meta-ophiolites

These can be divided into two complexes: (1) Nourabad and (2) Chehar-cheshmeh. The Nourabad complex (Virani is the older name) is exposed about 25 km west of Mashhad around the village of Nourabad (Fig. 1). The Chehar-cheshmeh meta-ophiolite complex is exposed between Vakilabad and Khlaj (Fig. 1). Hornblende gabbro (ophiolite) was dated by the $^{40}Ar–^{39}Ar$ method at 281.4 Ma and 277.4 Ma, with corresponding isochron ages of 287.6 and 281.7 Ma, suggesting Late Pennsylvanian – Early Permian ages, similar to other ages for Paleo-Tethys oceanic crust (Ghazi et al., 2001).

According to detailed studies by Alavi (1979, 1991, 1992), "meta-ophiolites" constitute allochthonous sheets which are displaced onto the surrounding flysch deposits by a low angle, precollisional ductile thrust system that is associated with mylonites and a mesoscopic sheared-off fault-drag fold. Mylonites are a few centimeters to a meter wide.

2.2. Metaflysch

The metasedimentary rocks comprise slate, quartzite, marble, minor phyllite, and carbonate conglomerate and olistostromes. Alavi (1979) considered the metasedimentary rocks to represent deepwater flysch deposits. On the basis of Abbasi's (1998) research, the first stage of regional metamorphism was low pressure and medium temperature (staurolite zone within amphibolite facies).

The remnant Paleo-Tethys meta-ophiolite and associated metaflysch were intruded by the Dehnow diorite and Kuhsangi granodiorite.

2.3. Younger low-grade metasedimentary rocks

To the southwest of a major thrust fault (Fig. 1), there is a thick sequence of low-grade metamorphosed shale and with basal conglomerate. The conglomerate contains pebbles of ophiolite, metaflysch, diorite, and granodiorite. The basal conglomerate is highly sheared and silicified. Within the thrust zone there is a highly brecciated dolomite (Fig. 1). The shale contains plant fossils of Early Jurassic age. This second regional metamorphism must have occurred sometime after the emplacement of diorite and granodiorite.

Table 1
Major, trace and REE elements analysis of Dehnow–Vakilabd–Kuhsangi intrusive rocks.

Sample	59°24′38″	59°24′32″	59°26′51″	59°25′25″	59°25′27″	59°33′26″	59°27′05″
location	36°21′42″	36°21′44″	36°20′28″	36°19′31″	36°19′32″	36°14′42″	36°19′50″
Sample no.	1	2	3	4	5	6	7
Rock type	Diorite	Diorite	Granodiorite	Granodiorite	Granodiorite	Granodiorite	Granodiorite
SiO2	59.32	55.12	64.41	64.83	63.70	63.97	65.24
TiO_2	0.62	0.92	0.47	0.48	0.51	0.51	0.57
Al_2O_3	17.59	19.02	16.51	15.96	16.85	17.16	15.39
Fe_2O_3	1.59	1.44	1.40	1.18	1.20	1.40	1.85
FeO	4.77	7.15	3.86	3.96	3.96	3.69	4.41
MnO	0.14	0.2	0.13	0.12	0.13	0.12	0.11
MgO	2.60	2.7	1.68	1.85	1.71	1.32	1.89
CaO	5.69	7.25	4.25	3.78	4.18	4.77	3.84
Na_2O	2.48	1.9	2.74	2.84	3.03	2.75	2.41
K_2O	2.62	2.07	2.80	2.92	2.56	2.81	3.05
P_2O_5	0.20	0.23	0.16	0.14	0.18	0.20	0.19
$H_2O^{(+)}$	1.34	1.9	1.2	1.68	1.14	1.18	1.26
Total	99.12	99.8	99.93	99.93	99.59	99.99	100.21
Rb	96	76	100	103.5	99	105	110.4
Sr	514	537	433	371	448	418	396
Ba	576	470	557	492	517	550	561
Nb	21.5	30.5	21.5	22.1	24.1	23.7	25.9
Zr	154	177	145	137	170	187	155
Ga	23	23.6	18	16	19	16	22
Rb/Sr	0.18	0.14	0.23	0.28	0.22	0.25	0.27
Rb/Ba	0.16	0.16	0.18	0.21	0.19	0.19	0.196
Fe_2O_3/FeO	0.33	0.2	0.29	0.27	0.28	0.29	0.41
La	28.06	37.2	30.17	20.81	37	55.5	37.94
Ce	58.9	78.2	62.58	44.62	79	114.9	85.97
Pr	6.22	8.31	6.57	4.69	8.11	11.91	8.51
Nd	22.31	29.6	21.88	17.37	30.7	40.6	30.55
Sm	4.83	5.12	3.8	3.81	5.26	5.58	6.05
Eu	1.37	1.27	0.89	1.23	1.3	1.39	1.55
Gd	3.85	3.86	3.33	2.91	4.37	3.28	4.24
Dy	3.66	2.61	3.52	2.79	3.72	1.41	2.93
Er	2.27	1.22	2.05	1.57	1.97	0.59	1.47
Y	18.7	22.4	21.2	14.3	15.4	14.1	15.4
Yb	1.77	1.17	2.3	1.35	1.95	0.58	1.23
$(La/Yb)_N$	19.69	21.32	10.02	10.39	12.86	21.32	20.8
Eu/Eu*	0.97	0.87	0.76	1.13	0.83	0.87	0.94

	59°24′32″ 36°21′44″	59°24′05″ 36°21′50″	59°27′45″ 36°19′45″	59°25′11″ 36°19′46″
	8	9	10	11
	Diorite	Diorite	Granodiorite	Granodiorite
SiO_2	58.16	55.1	64.74	63.49
TiO_2	0.76	0.96	0.48	0.51
Al_2O_3	18.14	18.65	16.42	16.84
Fe_2O_3	1.86	1.95	1.16	1.71
FeO	5.58	6.70	3.95	3.78
MnO	0.16	0.16	0.13	0.13
MgO	2.32	3.01	1.79	1.88
CaO	6.13	6.99	4.28	4.01
Na_2O	2.71	2.46	3.0	2.72
K_2O	2.76	2.02	2.69	2.64
P_2O_5	0.22	0.32	0.18	0.20
$H_2O^{(+)}$	1.4	1.7	1.2	1.35
Total	100.3	99.84	100.14	99.59
Rb	102	75	100	97
Sr	540	533	460	450
Ba	594	466	551	487
Nb	28.8	31.9	23.1	24
Zr	205	178	156	156
Ga	19	24	21	18
Rb/Sr	0.18	0.14	0.21	0.2
Rb/Ba	0.17	0.16	0.18	0.19
Fe_2O_3/FeO	0.33	0.33	0.29	0.29

2.4. Jurassic sedimentary rocks

A narrow, northwest-trending tectonic basin contains interlayered sandstone, shale, and siltstone with a basal conglomerate (Fig. 1). The basal conglomerate contains pebbles and cobbles of metaflysch, Dehnow diorite, and Kuhsangi granodiorite. There are thin coal-bearing horizons within the shale. Abundant plant fossils indicate that the age of this sequence is Lias–Dogger (Khatonie Molayossefi, 2000).

3. Analytical techniques

3.1. Bulk-rock chemistry

Fieldwork was carried out in the plutonic metamorphic belt for more than 10 years. Detailed field observations and petrographic study of more than 100 samples signified that the mineralogical compositions of both the granodiorite and diorite are very uniform. Previous major and trace element analysis also indicated that there is very little chemical variation within either the Dehnow or Kuhsangi intrusions. Therefore we selected only 11 samples, which we consider representative, for new analysis.

Major elements were analyzed by wavelength-dispersive X-ray fluorescence (XRF) spectrometry using fused discs and the Philips PW 1410 XRF spectrometer at Ferdowsi University, Mashhad, Iran. Pressed-powder pellets were used for Zr, Nb, Sn, Sr, Ba, Sc, Y, and Ga measurements by XRF. FeO and Fe_2O_3 contents were determined with precision of ±1% by titration with standardized potassium permanganate solution at Ferdowsi University of Mashhad, Iran.

The REE compositions of the samples were determined by inductively coupled plasma–mass spectrometry (ICP–MS) at Acme Analytical Laboratories, Vancouver, British Columbia, Canada.

3.2. Zircon U–Pb dating

Two rock samples, were analyzed for Sr and Nd isotopes, were chosen for zircon U–Pb age dating. About 70 zircons were isolated from each rock by using standard mineral separation techniques. The zircons were mounted along with a zircon standard and a couple of chips of NBS 610 Trace Element Glass in epoxy and polished down to 20 μm thickness. Zircon age dating was done at the Arizona LaserChron Center following the method of Gehrels and Valencia (2006). Cathode-luminescence (CL) images of the samples were acquired because such images (1) provide a powerful tool for placing the laser pits in homogeneous parts of the crystals and (2) can yield data on the origin (e.g., igneous, metamorphic, hydrothermal) of the zircon grains.

Laser ablation generally uses a beam diameter of either 35 or 25 μm; however, a beam diameter of 15 or 10 μm is used when finer spatial resolution was needed. With a 35- or 25-μm beam, the laser is set at a repetition rate of 8 Hz and energy of 100 mJ, which excavates at a rate of ~1 μm/s. This procedure generates a signal of ~100,000 cps per ppm for U in zircon. For smaller beam sizes, the ablation rate is reduced to ~0.5 μm/s by reducing the laser energy (60 mJ) and repetition rate (4 Hz). In both cases the ablated material is removed from the ablation chamber in He carrier gas. The carrier gas (and sample) are then mixed with Ar gas before entering the plasma of the ICP–MS.

Isotopic analysis is performed with a multicollector inductively coupled plasma–mass spectrometry (MC–ICP–MS: GVI Isoprobe) that is equipped with an S-option interface. The instrument is equipped with a collision cell that is operated with an argon flow rate of 0.2 mL/min to create a uniform energy distribution, and the accelerating voltage is ~6 kV. Collectors include nine Faraday detectors and four low-side channeltron multipliers, all of which are movable, as well as an axial Daly photomultiplier.

3.3. Sr and Nd isotopes

Sr and Nd isotopic analyses were performed on a six-collector Finnigan MAT 261 thermal-ionization mass spectrometer at the University of Colorado, Boulder, Colorado, United States. $^{87}Sr/^{86}Sr$ ratios were determined by using four-collector static mode measurements. Thirty measurements of SRM-987 during the study period yielded a mean $^{87}Sr/^{86}Sr = 0.71032 \pm 2$ (error is the 2σ mean). Measured $^{87}Sr/^{86}Sr$ ratios were corrected to SRM-987 = 0.71028. Measured $^{143}Nd/^{144}Nd$ was normalized to $^{146}Nd/^{144}Nd = 0.7219$. Analyses were made as dynamic mode, three-collector measurements. Thirty-three measurements of the La Jolla Nd standard during the study period yielded a mean $^{143}Nd/^{144}Nd = 0.511838 \pm 8$ (error is the 2σ mean).

4. Petrography

4.1. Dehnow diorite

The Dehnow diorite crops out in the northwestern part of the plutonic belt. Its composition ranges from hornblende biotite diorite to granodiorite (Fig. 1). The diorite contains 35–50% plagioclase, 10–14% K-feldspar, 9–14% quartz, 15–11% biotite, 2% hornblende and less than 2% accessory phases. Plagioclase has minor weak zoning. Quartz is anhedral and found as interstitial grains. Accessory minerals are apatite, zircon, and ilmenite. Xenoliths within the hornblende biotite diorite mainly represent the country rocks such as slates, meta-peridotite, and meta-gabbro.

Large xenocrystic almandine garnets are found within the diorite near the northern contact where the country rocks are Fe-rich metapelite. The garnets, up to 2 cm in diameter, are not homogeneous. They contain inclusions of biotite, quartz, and plagioclase. Originally the xenocrysts were pieces of slate that were metamorphosed to garnet, biotite, quartz, and plagioclase.

Field observation shows that the diorite-granodiorite intruded the already-metamorphosed flysch after the first regional metamorphism (late Paleozoic). The diorite has a medium-grained hypidiomorphic texture. It commonly displays a weakly to moderately developed foliation. This foliation does not follow the intrusive contact and instead has a strike similar to that of the regional slaty cleavage. This fabric therefore appears to be a result of the second regional metamorphism, which occurred in the Jurassic.

4.2. Kuhsangi granodiorite

The granodiorite crops out in the area of Vakilabad and Kuhsangi (Fig. 1). The granodiorite contains 30–40% plagioclase, 13–18% K-feldspar, 15–27% quartz, and 7–10% biotite. Some plagioclase shows normal zoning. Quartz is anhedral and found as interstitial grains. Biotite is also anhedral. Common accessory minerals include apatite, zircon, and ilmenite. The granodiorite has medium- to fine-grained hypidiomorphic texture. The biotite shows very good foliation, which follows the slaty cleavage of the second regional metamorphism.

Field observation shows that the granodiorite intruded after the first regional metamorphism (late Paleozoic) and before the second regional metamorphism (Late Triassic–Early Jurassic).

5. Analytical results

5.1. Whole-rock geochemistry

Representative whole-rock major and trace element analyses for 11 diorite and granodiorite samples are listed in Table 1. A plot of $SiO_2/(K_2O + Na_2O)$ (Cox et al., 1979) shows that the Dehnow intrusive rocks plot in the field of diorite and the Kuhsangi (formerly Vakilabad) intrusive rocks plot in the field of granodiorite (Fig. 2). A plot of K_2O vs. SiO_2 (after Rickwood, 1989) shows that both intrusive rock types plot in the field of high-K sub-alkaline magmas (Fig. 3). The K_2O/Na_2O ratio is between 0.89 and 1.05.

A discrimination plot of Zr + Ce + Y + Nb vs. $(Na_2O + K_2O)/CaO$ (after Whalen et al., 1987) shows that the diorite and granodiorite plot within the field for I- and S-type granitoids (Fig. 4).

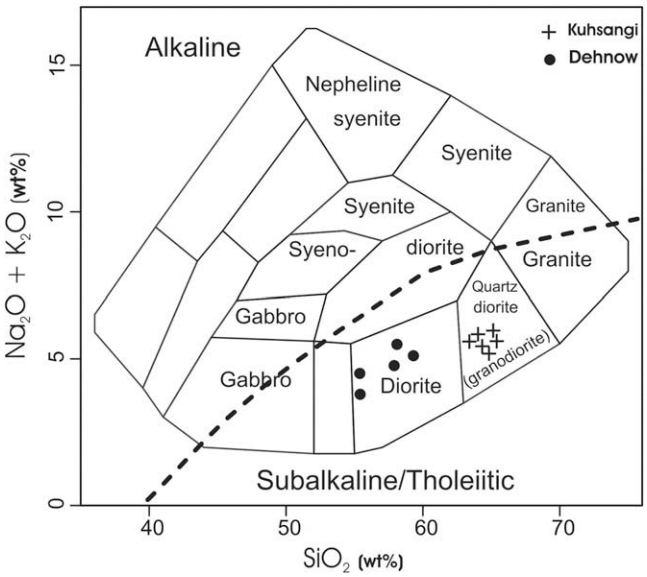

Fig. 2. Classification of Dehnow and Kuhsangi intrusive rocks (Cox et al., 1979).

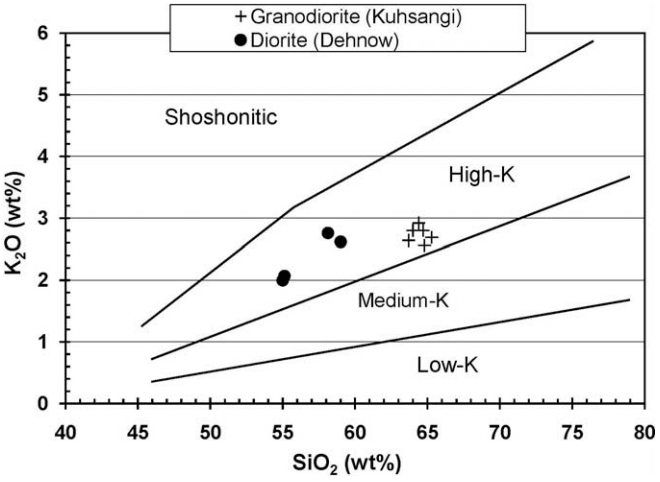

Fig. 3. K_2O vs. SiO_2 variation diagram (Rickwood, 1989) with boundaries by Peccerillo and Taylor (1976) for high-K, medium-K, and low-K magma series. The Dehnow and Kuhsangi intrusive rocks plot in the high-K field.

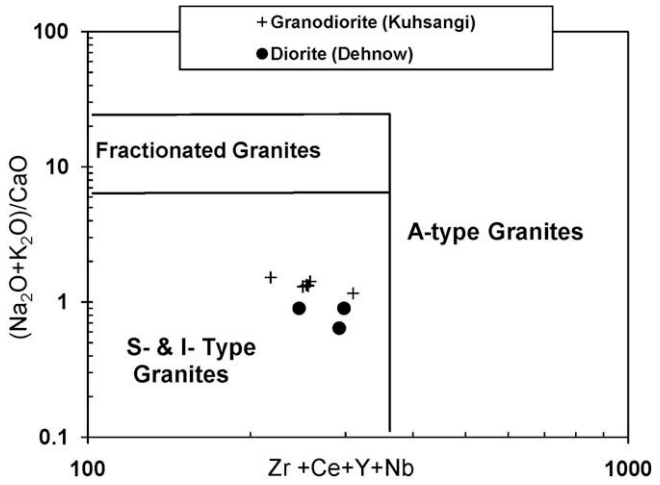

Fig. 4. Plot of (Zr + Ce + Y + Nb)/[(Na_2O + K_2O)/CaO]. The intrusive rocks plot in the field of I- and S-type granites (Whalen et al., 1987).

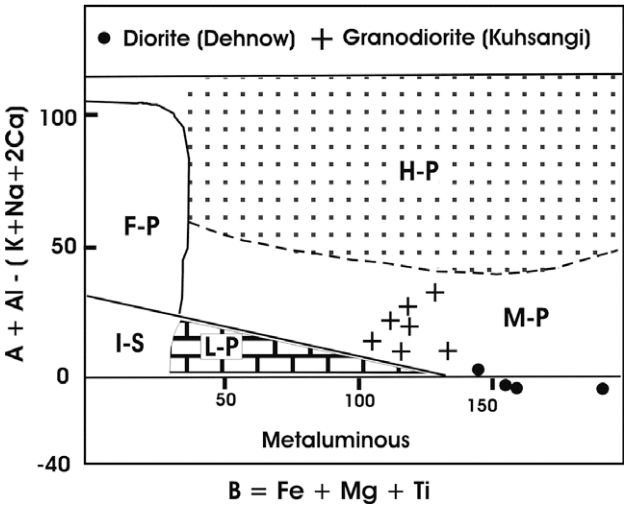

Fig. 5. The Dehnow and Kuhsangi intrusive rocks plot in the field of moderately peraluminous (M-P) granitoids (Villaseca et al., 1998). (L-P = low peraluminous; M-P = moderately peraluminous; H-P = highly peraluminous; F-P = felsic peraluminous).

Villaseca et al. (1998) divided peraluminous granites into four groups (Fig. 5): (1) Highly peraluminous granitoids (H-P), which are the typical S-type granites. They have the highest A = (Al/(K + Na + 2Ca). They are characterized by having Al-rich minerals such as muscovite, garnet (almandine-pyrope series), cordierite, and sillimanite. They usually contain abundant restitic enclaves. (2) Moderately peraluminous granitoids (M-P). These are biotite bearing. Accessory phases are cordierite and garnet (almandine-spessartine series). (3) Low peraluminous granitoids (L-P). These rocks could be evolved from I-type or the low-ASI-type granitoids. They may contain amphibole. Enclaves are mainly mafic granular types. (4) Highly felsic peraluminous granitoids (F-P).

The Dehnow diorite and Kuhsangi granodiorite plot in the field of moderately peraluminous granitoids (M-P). Because they plot above the I–S line, they are therefore S-type granitoids (Fig. 5).

5.2. Trace and rare earth elements (REEs)

The low field strength element (LFSE) (Rb, Ba, and Sr) content of the diorite and granodiorite are in general high (Table 1). The diorite has the lowest Rb ≈ 75–102 ppm (Table 1). The Rb/Sr is between 0.14 and 0.18 in the diorite and, 0.20 and 0.27 in the granodiorite (Table 1). The Ba content of both intrusive rocks is between 460 to 590 ppm (Table 1).

REE analyses (normalized with respect to chondrites (Boynton, 1984)) of selected samples from the diorite and granodiorite are shown in Table 1. In general, the diorite and granodiorite exhibit similar chondrite-normalized REE patterns (Fig. 6), which are characterized by moderate light rare earth element (LREE) enrichment and medium heavy REE (HREE) enrichment. The diorite and granodiorite have total rare earth contents of 100–180 ppm and La_N/Yb_N = 6.33–11.38. The ratios of Eu/Eu* vary from 0.74 to 1.1 (Taylor and McLennan, 1985). Therefore, these rocks have small negative or no Eu anomalies (Eu/Eu* < 1.0).

Chondrite-normalized spidergrams (Thompson, 1982) of representative samples of the diorite and granodiorite are plotted in Fig. 7. Well-defined negative anomalies are observed for P, Ti, Sr, and Nb. Fractionation or presence of some minerals in the restites explain the negative anomalies, for example, apatite (P) and ilmenite and/or titanite (Ti). The LFSE elements Ba and Rb show positive anomalies; Rb shows the highest positive anomaly (Fig. 7). The

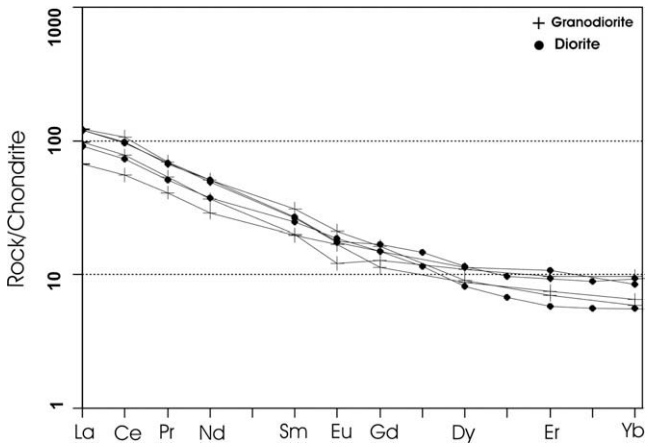

Fig. 6. Chondrite-normalized REE distribution (Boynton, 1984) for the Dehnow diorite and Kuhsangi granodiorite.

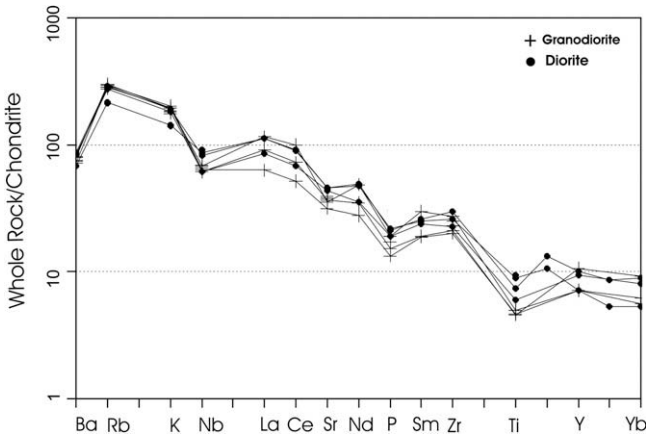

Fig. 7. Chondrite-normalized spidergrams (Thompson, 1982 of representative samples from the Dehnow diorite and Kuhsangi granodiorite.

high field strength elements (HFSEs) Zr and Ce show small positive anomalies (Fig. 7).

6. Magnetic susceptibility

Granitic rocks were classified into the magnetite series and the ilmenite series by Ishihara (1977). Ishihara recognized that in Japan there is a distinct spatial distribution of granitic rocks that contain magnetite coexisting with ilmenite and those that contain ilmenite as the only Fe-Ti oxide. He recognized that the magnetite series granitoids are relatively oxidized, whereas the ilmenite series granitoids are relatively reduced. Granites showing a magnetic susceptibility value of $>3.0 \times 10^{-3}$ (SI units) are classified as belonging to the magnetite series (Ishihara, 1981). The magnetic susceptibility and the Fe_2O_3/FeO (bulk chemistry of rocks) ratio of granodiorite and diorites are reported in Table 2. These data, when plotted against each other, indicate that the granodiorite and diorite belong to the ilmenite series (Fig. 8a).

On the basis of mineralogy, Iranmanesh and Sethna (1998) classified the Dehnow diorite and Kuhsangi granodiorite as I-type granites belonging to the magnetite series. Both of these classifications are incorrect. Magnetic susceptibility, mineralogical composition, and the ferric to ferrous ratio (<0.35) of the Dehnow diorite and Kuhsangi granodiorite require that they belong to the ilmenite series. Their mineralogical-chemical composition (Figs. 5 and 8b) and initial $^{87}Sr/^{86}Sr$ and $^{143}Nd/^{144}Nd$ ratios (0.707949–0.708589 and 0.512059–0.512019, respectively) also indicate that they are S-type granitoids.

The classification of the magnetite series and ilmenite series granitoids plus their Rb/Sr ratios are very powerful tools in mineral

Table 2
Magnetic susceptibility of Dehnow–Vakilabd–Kuhsangi intrusive rocks (Diorite-granodiorite).

Sample no.	X	Y	Magnetic susceptibility 10^{-5} SI	Fe_2O_3/FeO (wt.%)
1	59°24′38″	36°21′42″	9	0.33
2	59°24′32″	36°21′44″	16	0.2
3	59°26′51″	36°20′28″	17	0.29
4	59°25′25″	36°19′31″	23	0.27
5	59°25′27″	36°19′32″	19	0.22
6	59°33′′26″	36°14′42″	13	0.25
7	59°27′05″	36°19′50″	5	0.41
8	59°24′19″	36°21′46″	6	0.33
9	59°24′05″	36°21′50″	9	0.33
10	59°27′45″	36°19′45″	9	0.29
11	59°25′11″	36°19′46″	13	0.2
12	59°24′31″	36°21′32″	15	0.31
13	59°33′28″	36°16′41″	8	0.29
14	59°25′15″	36°19′45″	9	0.42
15	59°33′30″	36°16′41″	19	0.29

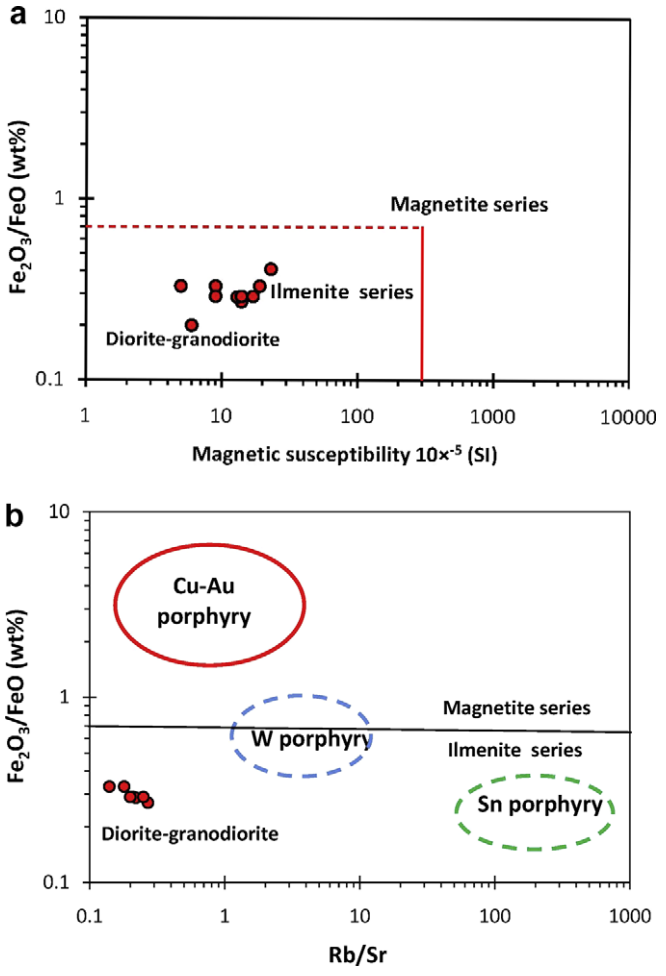

Fig. 8. (a) A plot of magnetic susceptibility vs. Fe_2O_3/FeO shows that the Dehnow and Kuhsangi intrusive rocks belong to the ilmenite series. (b) Plot of (Rb/Sr)/(FeO/F_2O_3) indicate that diorite and granodiorite have Low Rb/Sr and Fe_2O_3/FeO ratios.

Table 3
Results of U–Pb–Th laser-ablation multicollector ICP mass spectrometry analysis of zircon from Dehnow diorite and Kuhsangi granodiorite.

Analysis	U (ppm)	$^{206}Pb/^{204}Pb$	U/Th	$^{206}Pb/^{207}Pb$	± (%)	$^{207}Pb/^{235}U$	± (%)	$^{206}Pb/^{238}U$	± (%)	Age (Ma)	± (Ma)
Granodiorite Kuhsangi (sample no. 6)											
1	151	952	1.4	14.8919	14.5	0.3291	14.6	0.0355	1.1	225.2	2.5
2	249	6102	2.3	19.9499	3.5	0.2342	4.2	0.0339	2.4	214.8	5.1
3	502	5806	3.0	19.5585	2.7	0.2393	2.8	0.0340	0.8	215.2	1.7
4	883	3738	3.9	18.0135	5.4	0.2617	5.5	0.0342	0.8	216.7	1.7
5	206	3700	2.3	18.6108	7.6	0.2527	8.8	0.0341	4.3	216.3	9.2
6	335	9464	1.7	20.5926	4.2	0.2256	4.3	0.0337	1.0	213.6	2.0
7	366	12,286	2.1	20.2815	3.0	0.2302	5.2	0.0339	4.3	214.7	9.0
8	303	9948	2.2	20.0799	1.7	0.2399	2.4	0.0349	1.7	221.4	3.6
9	216	6332	1.6	19.2525	2.9	0.2434	3.3	0.0340	1.6	215.5	3.3
10	303	2590	2.1	19.3393	2.2	0.2443	4.3	0.0343	3.6	217.2	7.8
11	409	3956	2.5	18.4774	5.6	0.2530	7.6	0.0339	5.2	215.0	10.9
12	300	9178	1.8	19.2202	2.8	0.2446	3.7	0.0341	2.3	216.1	5.0
13	369	10,064	1.8	20.2104	3.2	0.2281	3.5	0.0334	1.5	212.0	3.2
14	372	5662	2.0	19.7046	3.0	0.2247	3.6	0.0321	2.1	203.8	4.3
15	233	6184	2.7	20.1721	2.4	0.2408	3.5	0.0352	2.6	223.2	5.6
16	479	15,704	2.5	20.1365	2.0	0.2386	3.6	0.0348	3.1	220.8	6.6
17	548	4514	3.3	18.8040	1.7	0.2558	2.0	0.0349	1.1	221.1	2.3
18	257	2778	2.8	18.4766	5.9	0.2646	6.0	0.0355	1.2	224.6	2.7
Diorite (Dehnow) (sample no. 2)											
1	448	17,148	2.4	20.0809	3.9	0.2259	4.2	0.0329	1.6	208.7	3.3
2	580	8590	3.7	19.2134	2.8	0.2410	3.3	0.0336	1.6	213.0	3.4
3	428	3682	4.0	19.1118	8.4	0.2438	8.4	0.0338	1.2	214.3	2.5
4	553	19,160	3.8	19.8499	1.6	0.2343	2.4	0.0337	1.8	213.9	3.8
5	548	32,376	4.4	20.3273	3.5	0.2307	4.5	0.0340	2.8	215.6	5.9
6	801	16,410	3.6	19.4604	3.2	0.2397	3.5	0.0338	1.5	214.5	3.1
7	588	14,906	2.8	19.8105	3.6	0.2357	3.7	0.0339	0.9	214.7	1.9
8	604	18,492	4.1	19.8692	3.0	0.2349	4.3	0.0339	3.1	214.6	6.6
9	313	9218	5.3	19.7691	3.7	0.2373	4.0	0.0340	1.4	215.7	3.1
10	579	21,458	3.7	19.8940	2.8	0.2344	3.2	0.0338	1.6	214.4	3.3
11	416	11,596	5.8	19.9132	1.9	0.2290	2.4	0.0331	1.4	209.7	2.9
12	226	11,626	3.5	19.7561	3.4	0.2396	3.8	0.0343	1.7	217.6	3.7
13	266	9052	2.9	19.8609	3.7	0.2372	3.8	0.0342	1.0	216.6	2.1
14	421	7734	5.8	19.3885	6.7	0.2373	7.0	0.0334	2.3	211.6	4.7
15	428	13,892	2.6	19.5856	3.1	0.2346	3.8	0.0333	2.1	211.3	4.4
16	665	16,080	3.6	19.7714	1.4	0.2327	1.5	0.0334	0.5	211.6	1.0
17	253	6048	3.4	19.5864	2.9	0.2443	3.2	0.0347	1.2	220.0	2.7
18	696	34,236	3.4	19.7746	2.9	0.2360	3.8	0.0338	2.5	214.6	5.3
19	356	10,920	2.7	19.7648	2.9	0.2362	3.3	0.0339	1.5	214.6	3.2
20	298	2706	4.4	18.9095	9.4	0.2450	9.9	0.0336	3.3	213.0	7.0
21	488	17,136	3.9	19.5757	1.3	0.2348	1.8	0.0333	1.2	211.4	2.5

exploration. Intrusive rocks associated with Cu–Au porphyries are relatively oxidizing, and they have low Rb/Sr ratios (Fig. 8b). Porphyry Sn deposits are associated with reduced intrusive rocks with very high Rb/Sr ratio (Fig. 8b). Because the plot of Fe_2O_3/FeO vs. Rb/Sr ratios (Fig. 8b) shows that the Dehnow diorite and Kuhsangi granodiorite plot in the reduced (ilmenite series) field and have low Rb/Sr ratios, these rocks do not have any potential for Cu-Au, Sn, or Mo mineralization.

6.1. U–Th–Pb zircon age dating

The ophiolite that is a remnant of e Paleo-Tethys ocean was dated by Ghazi et al. (2001) using two methods: (1) ^{40}Ar–^{39}Ar, which gave ages of 281.4 and 277.4 Ma, and (2) K-Ar, which gave ages of 273 and 265 Ma. Both methods thus suggested Late Pennsylvanian – Early Permian ages.

In Iran, Turkey, and Greece, the Paleo-Tethys closure did not take place before the beginning of the Late Triassic (231 Ma). By the end of the Late Triassic (about 225 Ma), the Paleo-Tethys ocean certainly had closed in the area that is now Iran (Stampfli, 1996, 2002; Stampfli and Pillevuit, 1993; Stampfli et al., 1991; Davoudzadeh and Schmidt, 1984).

In an earlier study, Majidi (1983) dated the Dehnow diorite and Kuhsangi granodiorite by using the K-Ar method, which yielded ages of 256–245 Ma. Because these plutonic rocks were intruded during the closure of the Paleo-Tethys, their age must be younger than 225 Ma. Therefore the K-Ar age reported by Majidi is incorrect.

Two rock samples, which were analyzed for Sr and Nd isotopes, were chosen for U–Pb–Th dating of zircon. The U–Th–Pb dating was done at the Department of Geosciences, University of Arizona, Tucson, Arizona, United States.

The results of the U–Th–Pb zircon analysis of the two samples (No. 6—Kuhsangi granodiorite and No. 2—Dehnow diorite) are presented in Table 3.

The results of the calculation of the isotopic age of the Kuhsangi granodiorite are presented as concordia and TuffZirc graphics (Figs. 9a and b). On the basis of 18 analyzed points, the mean age (weighted mean) is 217 ± 4 Ma (errors shown are 2σ).

The results of the calculation of isotopic age of the Dehnow diorite are presented as concordia and TuffZirc graphics (Figs. 10a and b). On the basis of 21 analyzed points, the mean age (weighted mean) is 215 ± 4 Ma (errors shown are 2σ).

Therefore, the U–Th–Pb zircon age dating indicates that the Dehnow diorite and Kuhsangi granodiorite formed in Late Triassic (Norian) time.

6.2. Sr and Nd isotopes

Sr and Nd isotope data for representative samples are given in Table 4. Their initial $^{87}Sr/^{86}Sr$ and $^{143}Nd/^{144}Nd$ ratios range from 0.707949 to 0.708589 and from 0.512059 to 0.512019,

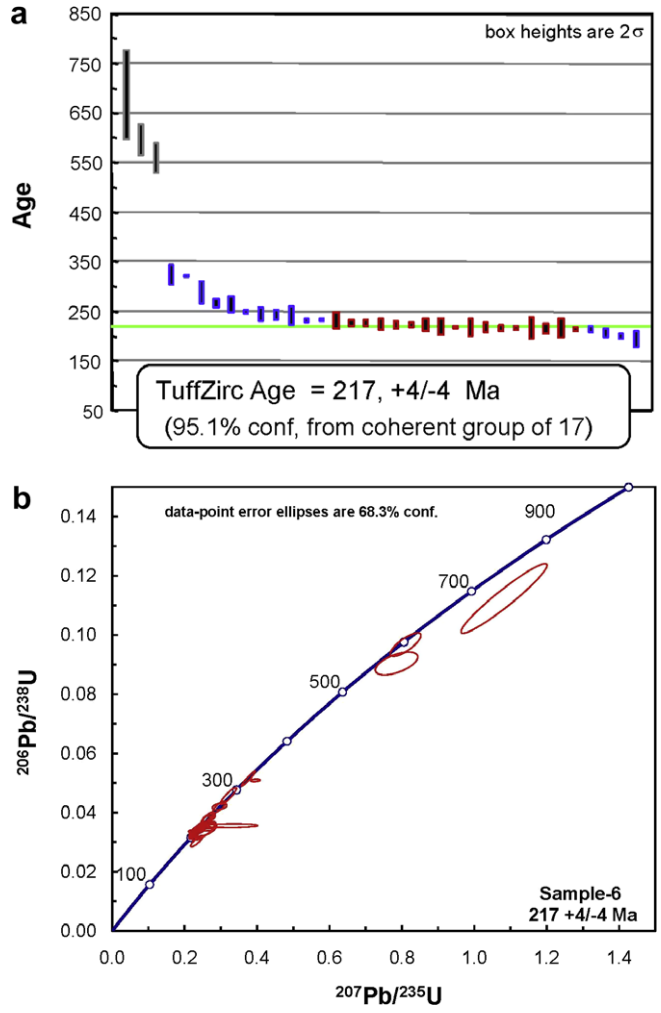

Fig. 9. (a) Concordia plot of $^{207}Pb/^{235}U$ vs. $^{206}Pb/^{238}U$ for calculating the age of zircons (Kuhsangi granodiorite). (b) TuffZirc plot shows the age of zircons from the Kuhsangi granodiorite.

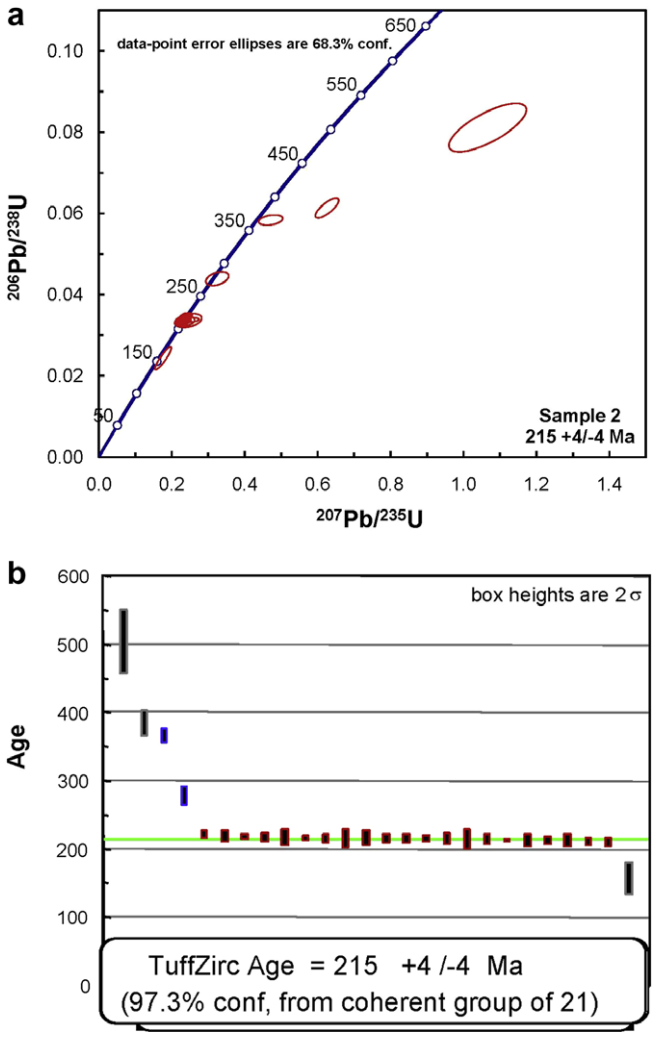

Fig. 10. (a) Concordia plot of $^{207}Pb/^{235}U$ vs. $^{206}Pb/^{238}U$ for calculating the age of zircons (Dehnow diorite). (b) TuffZirc plot shows the age of zircons from the Dehnow diorite.

respectively, when recalculated to an age of 217 Ma, consistent with the new radiometric results (Table 4). Initial ε_{Nd} isotope values for the Dehnow diorite and Kuhsangi granodiorite range from −6.63 to −5.90. The initial ε_{Nd} value of the slate is −13.79 (Table 4). The values for the plutonic rocks could be considered as representative of a continental crust–derived magma.

7. Discussion

7.1. Source of magma

Magnetic susceptibilities of the diorite and granodiorite are between 5×10^{-5} and 20×10^{-5} (SI units); therefore these rocks belong to the ilmenite series of reduced-type granitoids. They are also moderately peraluminous. The initial $^{87}Sr/^{86}Sr$, ε_{Nd}, and $^{143}Nd/^{144}Nd$ values of MORB basalts and of diorite, granodiorite, and slate from the study area are plotted in Fig. 11. The initial ε_{Nd} isotope values for the Dehnow diorite and Kuhsangi granodiorite range from −6.63 to −5.90, compared to MORB for which the value is between +7 and +13. The initial $^{87}Sr/^{86}Sr$ isotope values for the Dehnow diorite and Kuhsangi granodiorite range from 0.707949 to 0.708589, whereas the value for MORB is less than 0.704. Initial $^{143}Nd/^{144}Nd$ isotope ratios for the Dehnow diorite and Kuhsangi granodiorite range from 0.512059 to 0.512019; those for MORB are between 0.5130 and 0.5135. The isotope values thus indicate that both the diorite and the granodiorite did not originate in the mantle.

Following the collision of the Iranian and Turan plates, crustal shortening and thickening occurred. In continental collision zones, thickening of continental crust allows melting of metapelites, metagreywackes, and meta-igneous rocks under hydrated conditions. Such melting can produce silicic to intermediate-composition magmas of different series (i.e., Miller, 1985; Petford and Atherton, 1996). However, the initial $^{87}Sr/^{86}Sr$ isotope values of the Dehnow diorite and Kuhsangi granodiorite (0.708589) is different from the value shown by the slate (0.719306). This difference indicates that although the source of magma was in continental crust, the source was not solely the slate-related rock types.

The discrimination diagram that plots Rb/Sr vs. Rb/Ba ratios (Fig. 12) (Sylvester, 1998) shows that the Dehnow diorite and Kuhsangi granodiorite samples plot next to melt derived from metagreywacke. Dehydration–melting behavior of biotite in metapelitic rocks has been investigated by many workers, including Thompson (1982), Le Breton and Thompson (1988), Vielzeuf and Holloway (1988), Peterson and Newton (1989), Holtz and Johannes (1991), Patiño-Douce and Johnston (1991), Gardien et al. (1995), Patiño-Douce and Harris (1998), Annen et al. (2006), and Jagoutz et al. (2007). The amount and composition of

Table 4
Rb–Sr and Sm–Nd isotopic data of diorite (Dehnow) and granodiorite (Kuhsangi).

Sample	Rb (ppm)	Sr (ppm)	$^{87}Rb/^{86}Sr$	$(^{87}Sr/^{86}Sr)$ m (2σ)	R0(Sr)	Sm ppm	Nd ppm	$^{147}Sm/^{144}Nd$	$(^{143}Nd/^{144}Nd)$ m (2σ)	R0(Nd)	εNd I
Diorite sample (6)	100.1	438	0.6609	0.70997 (1)	0.70794	3.8	14.2	0.1614	0.512286 (12)	0.512059	−5.90
Granodiorite sample (2)	95.2	382	0.7198	0.71081 (1)	0.70859	5.75	32.5	0.1070	0.512171 (09)	0.512019	−6.63
Si-1(Slate)	149	74.8	5.7365	0.73701 (1)	0.71252	8.20	44.4	0.1116	0.511748 (07)	0.511590	−15.01

m = measured. Errors are reported as 2σ (95% confidence limit).
R0(Sr) is the initial ratio of $^{87}Sr/^{86}Sr$ for each sample, calculated using $^{87}Rb/^{86}Sr$ and $(^{87}Sr/^{86}Sr)$m and an age of 214.4 Ma (diorite) and 216.7 Ma (granodiorite) (age based on zircon).
R0(Nd) is the initial ratio of $^{143}Nd/^{144}Nd$ for each sample, calculated using $^{147}Sm/^{144}Nd$ and $(^{143}Nd/^{144}Nd)$m and an age of 214.4 Ma (diorite) and 216.7 Ma (granodiorite) (age based on zircon).
εNdI, initial εNd value.

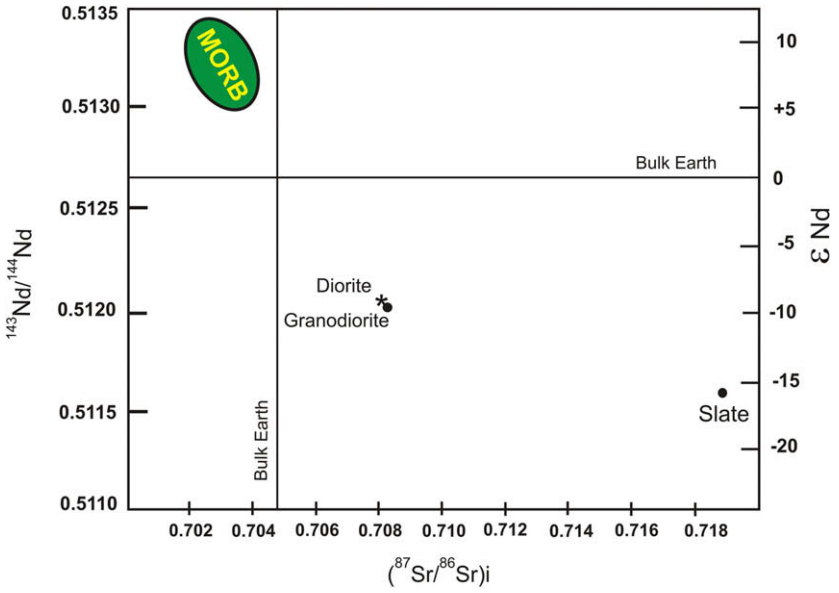

Fig. 11. Plot of initial $(^{87}Sr/^{86}Sr)_i$ vs. $^{143}Nd/^{144}Nd$ ratios.

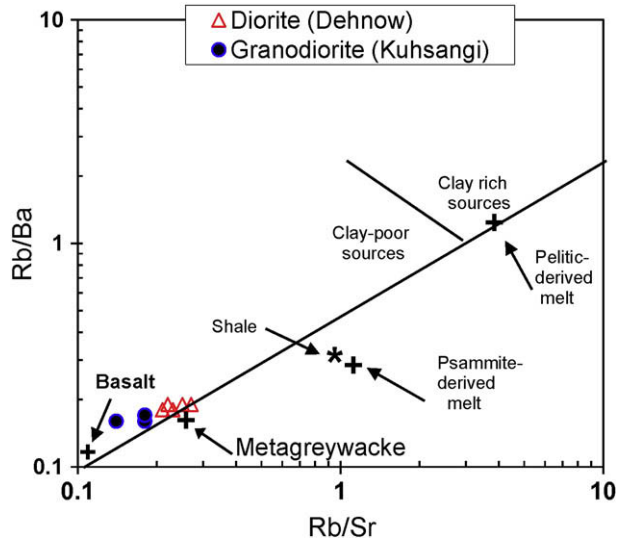

Fig. 12. Discrimination diagram of Rb/Sr vs. Rb/Ba (Sylvester, 1998). The Dehnow diorite and Kuhsangi granodiorite ratios plot near metagreywacke.

melts produced are dependent on various factors: composition of the source rocks, temperature, water content, pressure, and oxygen fugacity. In general, as the melts produced at low melting fractions are indistinguishable (mainly peraluminous) irrespective of the nature of the protolith, only the amount of melt will be different. Even metaluminous meta-igneous rocks—such as reported by Conrad et al. (1988), Beard et al. (1993), Beard and Lofgren (1991), Patiño-Douce and Beard (1995), and Springer and Seck (1997)—are able to produce peraluminous felsic melts at low melting fractions and in water-deficient conditions. As the melting increases, primary components of the source rocks are progressively incorporated into the melt. The Ti and Mg contents of biotite directly control the reaction temperature interval in biotite. As these elements increase in biotite, the reaction temperature interval will expand.

The Dehnow diorite and Kuhsangi granodiorite have low SiO_2, high Al_2O_3 (>15 wt.%), and low La_N/Yb_N = 6.33–21.32. Diorite or granodiorite with La_N/Yb_N = 6.33–21.32 must have originated from a depth and sources in which garnet was not present. The geophysical measurement carried out by Kunin (1987) indicated that the thickness of the continental crust in Binaloud area is between 48 and 50 km. The Dehnow diorite and Kuhsangi granodiorite therefore originated from a depth of less than 50 km.

8. Conclusions

The Paleo-Tethys ophiolite and metaflysch remnants were intruded by Dehnow biotite diorite and Kuhsangi granodiorite. These rocks contain up to 12% biotite, and they are moderately

peraluminous S-type granitoids. Their magnetic susceptibilities are between 5×10^{-5} and 20×10^{-5} (SI units); therefore they are classified as belonging to the reduced-type ilmenite series. The age of the Kuhsangi granodiorite based on zircon U–Pb age dating is 217 ± 4 Ma, and that of the Dehnow diorite is 215 ± 5 Ma (Late Triassic, Norian). The ranges of their initial $^{87}Sr/^{86}Sr$ and $^{143}Nd/^{144}Nd$ ratios are 0.707949–0.708589 and 0.512059–0.512019, respectively, when recalculated to an age of 217 Ma, consistent with the new radiometric results. The initial ε_{Nd} isotope values for the Dehnow diorite and Kuhsangi granodiorite range from −6.63 to −5.90. The initial ε_{Nd} isotope value for slate is −15.01. The values of the igneous rocks could be considered as representative of a continental crust–derived magma. Based on the geophysical measurement carried out by Kunin (1987), the thickness of the continental crust in the Binaloud area is between 48 and 50 km. Therefore, the Dehnow diorite and Kuhsangi granodiorite originated from a depth of less than 50 km. Melt derived from metagreywacke to metapelitic rocks is considered to have been the source of these granitoids.

Acknowledgements

This research was supported by Ferdowsi University of Mashhad, Iran (grant P/742-87/7/14). George E. Gehrels and Victor Valencia from the Department of Geosciences, University of Arizona, Tucson, Arizona, did the U–Th–Pb zircon age dating. The paper benefited greatly from reviews by K.N. Pang and M.H. Zarrinkoub.

References

Abbasi, H., 1998. Petrology of regional and contact metamorphic rocks south of Mashhad. M.Sc. thesis. Tehran University.

Alavi, M., 1979. The Virani ophiolite complex and surrounding rocks. Geologische Rundschau 68, 334–341.

Alavi, M., 1991. Sedimentary and structural characteristics of the Paleo-Tethys remnants in northeastern Iran. Geological Society of America Bulletin 103 (8), 983–992.

Alavi, M., 1992. Thrust tectonics of the Binaloud region: NE Iran. Tectonics 11 (2), 360–370.

Alberti, A., Moazez, Z., 1974. Plutonic and metamorphic rocks of the Mashhad area (northeastern Iran, Khorasan). Bollettino della Società Geologica Italiana 93, 1157–1196.

Annen, C., Bluny, J.D., Sparks, R.S.J., 2006. The genesis of intermediate and silicic magmas in deep crustal hot zones. Journal of Petrology 47 (3), 505–539.

Beard, J.S., Lofgren, G.E., 1991. Dehydration melting and water-saturated melting of basaltic andesitic greenstones and amphibolites at 1, 3, and 6.5 kb. Journal of Petrology 32, 365–401.

Beard, J.S., Abitz, R.J., Lofgren, G.H., 1993. Experimental melting of crustal xenoliths from Kilbourne Hole, New Mexico and implication for the contamination and genesis of magmas. Contributions to Mineralogy and Petrology 115, 88–103.

Boynton, W.V., 1984. Cosmochemistry of the rare earth elements: meteorite studies. In: Henderson, P. (Ed.), Rare Earth Element Geochemistry. Elsevier Sci Publ. Co., Amsterdam, pp. 63–114.

Conrad, W.K., Nicholls, I.A., Wall, V.J., 1988. Water-saturated and undersaturated melting of meta-aluminous and per-aluminous crustal compositions at 10 kb: evidence for the origin of silicic magmas in the Taupo volcanic zone, New Zealand, and other occurrences. Journal of Petrology 29, 765–803.

Cox, K.G., Bell, J.D., Pankhurst, R.J., 1979. The Interpretation of Igneous Rocks. Allen and Unwin, London. 450 p.

Davoudzadeh, M., Schmidt, K., 1984. Plate tectonics, orogeny, and mineralization in the Iranian fold belts. Report of a German–Iranian Research Program 1977-19, Neues Jahrbuch für Geologie und Paläontologie Abhandlungen, vol. 168, pp. 2–3, 182–207.

Gardien, V., Thompson, A.B., Grujic, D., Ulmer, P., 1995. Experimental melting biotite + quartz Muscovite assemblages and implications for crustal melting. Journal of Geophysical Research 100 (B8), 15581–15591.

Gehrels, G.E., Valencia, V., 2006. A Pullen in geochronology: emerging opportunities. In: T. Loszewski and W. Huff (Eds.), Paleontology Society. Short Course, vol. 12, pp. 67–76.

Ghazi, M., Hassanipak, A.A., Tucker, P.J., Mobasher, K., 2001. Geochemistry and $^{40}Ar–^{39}Ar$ ages of the Mashhad Ophiolite, NE Iran. Eos, Transactions, American Geophysical Union 82(47). Fall Meeting.

Holtz, F., Johannes, W., 1991. Genesis of peraluminous granites. I. Experimental investigation of melt compositions at 3 and 5 k bar and various H_2O activities. Journal of Petrology 32, 935–958.

Iranmanesh, J., Sethna, S.F., 1998. Petrography and geochemistry of the Mesozoic granite at Mashhad, Khorasan Province, northeastern part of Iran. Geological Society Journal of India 52 (1), 87–94.

Ishihara, S., 1977. The magnetite-series and ilmenite-series granitic rocks. Mining Geology 27, 293–305.

Ishihara, S., 1981. The Granitoid Series and Mineralization: Economic Geology. 75th Anniversary volume, pp. 458–484.

Jagoutz, O., Müntener, O., Ulmer, P., Pettke, T., Burg, J.P., Dawood, H., Hussain, S., 2007. Petrology and mineral chemistry of lower crustal intrusions: the Chilas complex, Kohistan (NW Pakistan). Journal of Petrology 48, 1895–1953.

Jarchovski, T., Momenzadeh, M., Tadayon, A., Ziegler, V., 1973. Mineral reconnaissance in Mashhad Quadrangle. Geological Survey of Iran, 192.

Khatonie Molayossefi, M., 2000. The study of stratigraphy and plants fossils of Shemshak formation in Shandiz area. M.Sc. thesis.

Kunin, N., 1987. Map of Depth to Moho. Institute of Physics of the Earth, Moscow.

Le Breton, N., Thompson, A.B., 1988. Fluid-absent (dehydration) melting of biotite in metapelites in the early stages of crustal anatexis. Contributions to Mineralogy and Petrology 99, 226–237.

Majidi, B., 1983. The geochemistry of ultrabasic and basic lava flows occurrences in northeastern Iran. In: Geodynamic Project in Iran. Geological Survey of Iran Report No. 51, pp. 463–477.

Miller, J.M., 1985. Are strongly peraluminous magmas derived from pelitic sedimentary sources. Journal of Geology 93, 673–689.

Mirnejad, H., 1991. Geochemistry and petrography of Mashhad granites and pegmatites. M.Sc. thesis, Tehran University.

Patiño-Douce, A.E., Beard, J.S., 1995. Dehydration–melting of biotite gneiss and quartz amphibolites from 3 to 15 k bar. Journal of Petrology 36, 707–738.

Patiño-Douce, A.E., Harris, N., 1998. Experimental constraints on Himalayan anatexis. Journal of Petrology 39, 689–710.

Patiño-Douce, A.E., Johnston, D.A., 1991. Phase equilibria and melt productivity in the pelitic system: implication for the origin of peraluminous granitoids and aluminous granulites. Contributions to Mineralogy and Petrology 107, 202–218.

Peccerillo, A., Taylor, S.R., 1976. Geochemistry of Eocene calc-alkaline volcanic rocks from the Kastamonu area, Northern Turkey. Contributions to Mineralogy and Petrology 58, 63–81.

Peterson, J.W., Newton, R.C., 1989. Reversed experiments on biotite–quartz–feldspar melting in the system KMASH: implications for crustal anatexis. Journal of Geology 97, 465–486.

Petford, N., Atherton, M., 1996. Na-rich partial melts from newly underplated basaltic crust: the cordillera blanca batholith, Peru. Journal of Petrology 37, 1491–1521.

Rickwood, P.C., 1989. Boundary lines within petrologic diagrams which use oxides of major and minor elements. Lithos 22, 247–267.

Springer, W., Seck, H.A., 1997. Partial fusion of basic granulites at 5–15 k bar: implication for the origin of TTG magmas. Contributions to Mineralogy and Petrology 127, 30–45.

Stampfli, G.M., 1996. The intra-alpine terrain: a Paleo-Tethyan remnant in the alpine variscides. Eclogae Geologicae Helvetiae 89 (1), 13–42.

Stampfli, G.M., 2000. Tethyan oceans. In: Bozkurt, E., Winchester, J.A., Piper, J.D.A. (Eds.), Tectonics and Magmatism in Turkey and Surrounding Area, vol. 173. Geological Society, Special Publication, London, pp. 163–185.

Stampfli, G.M., Marcoux, J., Baud, A., 1991. Tethyan margins in space and time. In: Channell, J.E.T., Winterer, E.L., Jansa, L.F. (Eds.), Paleogeography and paleoceanography of Tethys. Palaeogeography, Palaeoclimatology, Palaeoecology 87, 373–410.

Stampfli, G.M., Pillevuit, A., 1993. An alternative Permo-Triassic reconstruction of the kinematics of the Tethyan realm. In: J. Dercourt, L.-E. Ricou, and B. Vrielinck (Eds.), Atlas Tethys Palaeoenvironmental Maps. Explanatory Notes. Gauthier-Villars, Paris, 55–62.

Stocklin, J., 1974. Possible ancient continental margins in Iran. In: C.A. Burk, C.L. Drake (Eds.), The Geology of Continental Margins. pp. 873–887.

Sylvester, P.J., 1998. Post-collisional strongly peraluminous granites. Lithos 45 (1–4), 29–44.

Taylor, S.R., McLennan, S.M., 1985. The Continental Crust: Its Composition and Evolution. Blackwell Scientific Publication, Oxford.

Thompson, A.B., 1982. Dehydration melting of pelitic rocks and the generation of H_2O-undersaturated granitic liquids. American Journal of Science 282, 1567–1595.

Valizadeh, M., Karimpour, M.H., 1995. Origin and tectonic setting of Mashhad granitoids. Journal of Sciences, University of Tehran 21 (1), 71–82.

Vielzeuf, D., Holloway, J.R., 1988. Experimental determination of the liquid-absent melting relations in the pelitic system. Consequences for crustal differentiation. Contributions to Mineralogy and Petrology 98, 257–276.

Villaseca, C., Barbero, L., Herreros, V., 1998. A re-examination of the typology of peraluminous granite types in intra continental orogenic belts. Transactions of the Royal Society of Edinburgh: Earth Sciences 89, 113–119.

Whalen, J.B., Currie, K.L., Chappell, B.W., 1987. A-type granites: geochemical characteristics, discrimination and petrogenesis. Contributions to Mineralogy and Petrology 95, 407–419.